The Astrophysical Journal, 663:1040–1048, 2007 July 10
© 2007. The American Astronomical Society. All rights reserved. Printed in U.S.A.

A PANCHROMATIC STUDY OF THE GLOBULAR CLUSTER NGC 1904. I. THE BLUE STRAGGLER POPULATION[1]

B. Lanzoni,[2,3] N. Sanna,[4] F. R. Ferraro,[2] E. Valenti,[5] G. Beccari,[3,6,7] R. P. Schiavon,[8] R. T. Rood,[8] M. Mapelli,[9] and S. Sigurdsson[10]

Received 2007 February 23; accepted 2007 April 4

ABSTRACT

By combining high-resolution (*HST*/WFPC2) and wide-field ground-based (2.2 m ESO/WFI) and space (*GALEX*) observations, we have collected a multiwavelength photometric database (ranging from the far-UV to the near infrared) of the galactic globular cluster NGC 1904 (M79). The sample covers the entire cluster extension, from the very central regions up to the tidal radius. In the present paper, such a data set is used to study the BSS population and its radial distribution. A total number of 39 bright ($m_{218} \leq 19.5$) BSSs have been detected, and they have been found to be highly segregated in the cluster core. No significant upturn in the BSS frequency has been observed in the outskirts of NGC 1904, in contrast to other clusters (M3, 47 Tuc, NGC 6752, M5) studied with the same technique. Such evidence, coupled with the large radius of avoidance estimated for NGC 1904 ($r_{\rm avoid} \sim 30$ core radii), indicates that the vast majority of the cluster heavy stars (binaries) has already sunk to the core. Accordingly, extensive dynamical simulations suggest that BSSs formed by mass transfer activity in primordial binaries evolving in isolation in the cluster outskirts represent only a negligible (0%–10%) fraction of the overall population.

Subject headings: binaries: close — blue stragglers — globular clusters: individual (NGC 1904) — stars: evolution

1. INTRODUCTION

Blue straggler stars (BSSs) appear brighter and bluer than the turn-off (TO) point along an extension of the main sequence in color-magnitude diagrams (CMDs) of stellar populations. Hence, they mimic a young stellar population, with masses larger than the normal cluster stars (this is also confirmed by direct mass measurements; e.g., Shara et al. 1997). BSSs are thought to be objects that have increased their initial mass during their evolution, and two main scenarios have been proposed for their formation (e.g., Bailyn 1995): the *collisional scenario* suggests that BSSs are the end products of stellar mergers induced by collisions (COL-BSS), while in the *mass-transfer* scenario, BSSs form by the mass-transfer activity between two companions in a binary system (MT-BSS), possibly up to the complete coalescence of the two stars (Mateo et al. 1990; Pritchet & Glaspey 1991; Bailyn & Pinsonneault 1995; Carney et al. 2005; Tian et al. 2006; Leigh et al. 2007). Hence, understanding the origin of BSSs in stellar clusters can provide valuable insight into both the binary evolution processes and the effects of dynamical interactions on the (otherwise normal) stellar evolution. The MT formation scenario has recently received further support by high-resolution spectroscopic observations, which detected anomalous carbon and oxygen abundances on the surface of a number of BSSs in 47 Tuc (Ferraro et al. 2006b). However, the role and relative importance of the two mechanisms are still largely unknown.

To clarify the BSS formation and evolution processes, we are studying the BSS radial distribution over the entire cluster extension in a number of galactic globular clusters (GCs). We completed such studies in five GCs: M3 (Ferraro et al. 1997), 47 Tuc (Ferraro et al. 2004), NGC 6752 (Sabbi et al. 2004), ω Cen (Ferraro et al. 2006a), and M5 (Lanzoni et al. 2007; see also Warren et al. 2006). Apart from ω Cen, where mass segregation processes have not yet played a major role in altering the initial BSS distribution, the BSSs are always highly concentrated in the cluster central regions. Moreover, in M3, 47 Tuc, NGC 6752, and M5, the BSS fraction decreases at intermediate radii and rises again in the outskirts of the clusters, yielding a *bimodal* distribution. Preliminary evidence of such a bimodality has also been found in M55 by Zaggia et al. (1997). Recent dynamical simulations (Mapelli et al. 2004, 2006; Lanzoni et al. 2007) have been used to interpret the observed trends and have shown that a significant fraction ($\gtrsim$50%) of COL-BSSs is required to account for the observed BSS central peaks. In addition, a fraction of 20%–40% of MT-BSSs is needed to reproduce the outer increase observed in these clusters. The case of ω Cen is reproduced by assuming that the BSS population in this cluster is composed entirely of MT-BSSs. These results demonstrate that detailed studies of the BSS radial distribution within GCs are very powerful tools for better understanding the BSS formation channels and for probing the complex interplay between dynamics and stellar evolution in dense stellar systems.

In this paper, we present multiwavelength observations of NGC 1904. These observations are part of a coordinated project aimed at properly characterizing the UV excess of old stellar

[1] Based on observations with the NASA/ESA *HST*, obtained at the Space Telescope Science Institute, which is operated by AURA, Inc., under NASA contract NAS5-26555. Also based on *GALEX* observations (program GI-056) and WFI observations collected at the European Southern Observatory, La Silla, Chile, within the observing programs 62.L-0354 and 64.L-0439.

[2] Dipartimento di Astronomia, Università degli Studi di Bologna, via Ranzani 1, I-40127 Bologna, Italy.

[3] INAF-Osservatorio Astronomico di Bologna, via Ranzani 1, I-40127 Bologna, Italy.

[4] Dipartimento di Fisica, Università degli Studi di Roma Tor Vergata, via della Ricerca Scientifica, 1, I-00133 Roma, Italy.

[5] European Southern Observatory, Alonso de Cordova 3107, Vitacura, Santiago, Chile.

[6] Dipartimento di Scienze della Comunicazione, Università degli Studi di Teramo, Italy.

[7] INAF-Osservatorio Astronomico di Collurania, Via Mentore Maggini, I-64100 Teramo, Italy.

[8] Astronomy Department, University of Virginia, P.O. Box 400325, Charlottesville, VA 22904.

[9] University of Zürich, Institute for Theoretical Physics, Winterthurerstrasse 190, CH-8057 Zurich, Switzerland.

[10] Department of Astronomy and Astrophysics, The Pennsylvania State University, 525 Davey Lab, University Park, PA 16802.

aggregates as globular clusters, in terms of their hot stellar populations, such as horizontal-branch (HB) and extreme HB stars, post–asymptotic giant branch stars, BSSs, etc. From integrated light measurements obtained with the Ultraviolet Imaging Telescope (UIT; see Dorman et al. 1995), NGC 1904 was known to be relatively bright in the UV, and it was selected as a prime target in both our high-resolution (using *HST*) and wide-field (using *GALEX*) UV surveys. We have obtained a large set of data: (1) high-resolution ultraviolet (UV) and optical images of the cluster center have been secured with the WFPC2 on board *HST*; (2) complementary wide-field observations covering the entire cluster extension have been obtained in the UV and optical bands using the far- and near-UV detectors on board the *Galaxy Evolution Explorer* (*GALEX*) satellite and with ESO-WFI, mounted at the 2.2 m ESO telescope, respectively. The combination of these data sets allowed a study of the structural properties of NGC 1904 (thus leading to an accurate redetermination of the center of gravity and the surface density profile) and of the radial distribution of the evolved stellar populations (in particular the BSS and horizontal-branch star distributions have been derived over the entire cluster extension). While a companion paper (R. P. Schiavon et al. 2007, in preparation) will focus on the morphology and the structure of the HB, the present paper is devoted to the BSS population.

2. OBSERVATIONS AND DATA ANALYSIS

2.1. *The Data Sets*

The present study is based on a combination of different photometric data sets:

The high-resolution set.—This consists of a series of UV, near-UV, and optical images of the cluster center obtained with *HST*/WFPC2 with two different pointings. In both cases, the Planetary Camera (PC; the highest resolution instrument, with $0.046''$ pixel^{-1}) has been pointed approximately on the cluster center to efficiently resolve the stars in the highly crowded central regions; the three Wide Field Cameras (WFC; with resolution $0.1''$ pixel^{-1}) have been used to sample the surrounding regions. Observations in pointing A (Prop. 6607, PI: Ferraro) have been performed through filters F160BW (far-UV), F336W (approximately an *U* filter), and F555W (*V*), for a total exposure time $t_{\rm exp} = 3300$, 4400, and 300 s, respectively. Pointing B is a set of public *HST*/WFPC2 observations (Prop. 6095, PI: Djorgovski) obtained through filters F218W (mid-UV), F439W (*B*), and F555W (*V*). Because of the different orientations of the four cameras, this data set is complementary to the former (with the PC field of view in common), thus offering full coverage of the innermost regions of the cluster (see Fig. 1). The combined photometric sample is ideal for efficiently studying both the hot stellar populations (as the BSSs and the HB stars) and the cool red giant branch (RGB) population and guaranteeing a proper combination with the wide-field data set (see below).

The photometric reduction of both the high-resolution sets was carried out using `romafot` (Buonanno et al. 1983), a package developed to perform accurate photometry in crowded fields and specifically optimized to handle undersampled point spread functions (PSFs; Buonanno & Iannicola 1989), as in the case of the *HST*/WFC chips. The standard procedure described in Ferraro et al. (1997, 2001) was adopted to derive the instrumental magnitudes and to calibrate them to the STMAG system by using the zero points of Holtzman et al. (1995). The magnitude lists were finally cross-correlated in order to obtain a combined catalog.

The wide-field set.—A complementary set of wide-field *U*, *B*, and *I* images was secured by using the Wide Field Imager (WFI) at the 2.2 m ESO/MPI telescope, during an observing run in January 1999 (Program ID 062.L-0354, PI: Ferraro). A set of WFI *V* images (Program ID 064.L-0255) was also retrieved from the ESO/STECF Science Archive. Additional deep wide-field images were obtained in the UV band with the satellite *GALEX* (GI-056, PI: Schiavon) through the FUV (1350–1750 Å) and NUV (1750–2800 Å) detectors. With a global field of view (FoV) of $34' \times 34'$, the WFI observations cover the entire cluster extension. There is also full coverage of the cluster in the UV, thanks to the large *GALEX* FoV, which is approximately 1° in diameter and includes the WFI FoV (see Fig. 2, where the cluster is roughly centered on WFI CCD 2). However, because of the low resolution of the instrument ($4''$ and $6''$ in the FUV and NUV channels, respectively), *GALEX* data have been used to sample only the external cluster regions not covered by *HST*.

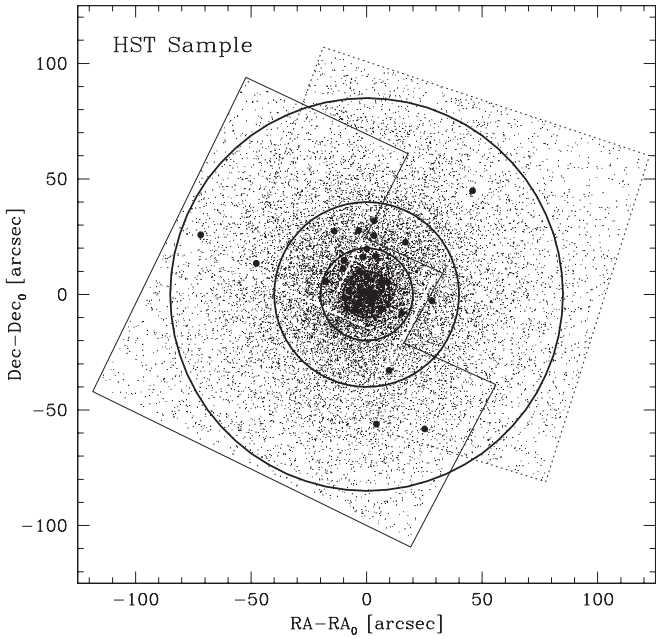


FIG. 1.—Map of the combined *HST* sample. The light solid and dotted lines delimit the FoVs of pointings B and A, respectively. Star positions are plotted with respect to the center of gravity $C_{\rm grav}$ derived in § 2.3: α(J2000.0) = $05^{\rm h}24^{\rm m}11.09^{\rm s}$, δ(J2000.0) = $-24^\circ 31' 29.00''$. The positions of all BSSs identified in this sample are marked with heavy dots, and the concentric annuli used to study their radial distribution (see Table 1) are also shown. The inner and outer annuli correspond to $r = r_c = 10''$ and $r = 85''$, respectively.

The raw WFI images were corrected for bias and flat field, and the overscan regions were trimmed using IRAF[11] tools (`mscred` package). Standard crowded field photometry, including PSF modeling, was carried out independently on each image using `daophotII/allstar` (Stetson 1987). For each WFI chip, a catalog listing the instrumental *U*, *B*, *V*, and *I* magnitudes was obtained by cross-correlating the single-band catalogs. Several hundred stars in common with Kravtsov et al. (1997), Stetson (2000),[12] and Ferraro et al. (1992) have been used to transform the instrumental *U*, *B*, *V*, and *I* magnitudes to the Johnson/Cousins photometric system.

For *GALEX* observations, as for the WFI data, standard photometry and PSF fitting were performed independently on each image using `daophotII/allstar`. A combined FUV-NUV

[11] IRAF is distributed by the National Optical Astronomy Observatory, which is operated by the Association of Universities for Research in Astronomy, Inc., under cooperative agreement with the National Science Foundation.

[12] For the photometric standards list, see http://cadcwww.hia.nrc.ca/standards/.

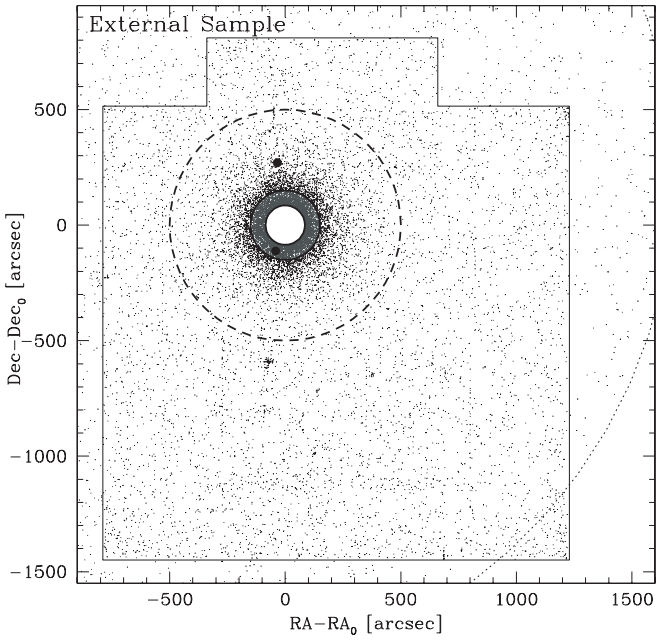


FIG. 2.—Map of the External sample. The light solid and dotted lines delimit the WFI and the *GALEX* FoVs, respectively. The two BSSs detected in the External sample are marked as heavy dots, and the concentric annuli used to study their radial distribution are shown as heavy circles. The inner annulus is at 85″ and corresponds to the most external one in Fig. 1. The heavy dashed circle marks the tidal radius of the cluster ($r_t \simeq 500''$).

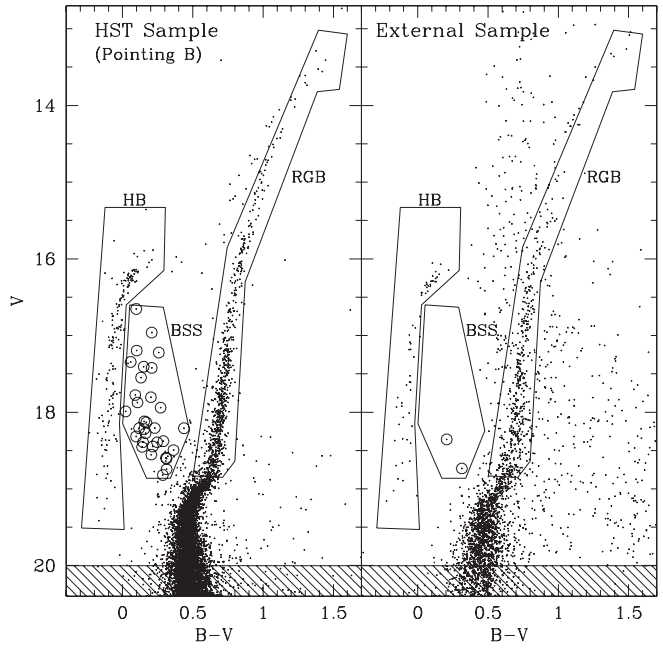


FIG. 3.—(V, $B-V$) CMDs of the *HST* (pointing B) and External samples. The hatched regions ($V \geq 20$) indicate the stars not used to derive the cluster surface density profile. The adopted BSS and HB selection boxes are shown, and all the identified BSSs are marked with open circles.

catalog was then obtained by cross-correlating the single-band catalogs.

2.2. *Astrometry and Homogenization of the Catalogs*

The *HST*, WFI, and *GALEX* catalogs have been placed on the absolute astrometric system by adopting the procedure already described in Ferraro et al. (2001, 2003). The new astrometric Guide Star Catalog (GSC-II)[13] was used to search for astrometric standard stars in the WFI FoV, and a cross-correlation tool specifically developed at the Bologna Observatory (P. Montegriffo et al. 2003, private communication) has been employed to obtain an astrometric solution for each WFI chip. Several hundred GSC-II reference stars were found in each chip, thus allowing an accurate absolute positioning of the stars. We then used more than 3000 and 1500 bright WFI stars in common with the *HST* and *GALEX* samples, respectively, as secondary astrometric standards, so as to place all the catalogs on the same absolute astrometric system. We estimate that the global uncertainties in the astrometric solution is of the order of $\sim 0.2''$, in both right ascension (α) and declination (δ).

Once placed on the same coordinate system, the catalogs were cross-correlated and the stars in common were used to transform all the magnitudes in the same photometric system. In particular, the *HST* STMAG magnitudes were converted to the WFI ones by using the stars in common between the two samples in the optical bands. The *GALEX* FUV and NUV instrumental magnitudes were then calibrated onto the *HST* m_{160} and m_{218} magnitudes, respectively, using the stars in common between the *GALEX* and *HST* samples. At the end of the procedure, a homogeneous master catalog of magnitudes and absolute coordinates of all the stars included in the *HST*, WFI, and *GALEX* samples was finally produced.

[13] Available at http://www-gsss.stsci.edu/Catalogs/GSC/GSC2/GSC2.htm.

2.3. *Center of Gravity and Definition of the Samples*

Once the absolute positions of individual stars have been obtained, the center of gravity $C_{\rm grav}$ of NGC 1904 is determined by averaging the coordinates α and δ of all stars lying in the PC FoV, following the iterative procedure described in Montegriffo et al. (1995; see also Ferraro et al. 2003, 2004). In order to correct for spurious effects due to incompleteness in the very inner regions of the cluster, we considered two samples with different limiting magnitudes ($V < 19$ and $V < 20$), and we computed the barycenter of stars for each sample. The two estimates agree within $\sim 1''$, setting $C_{\rm grav}$ at $\alpha({\rm J2000.0}) = 05^{\rm h}24^{\rm m}11.09^{\rm s}$, $\delta({\rm J2000.0}) = -24^{\rm o}31'29.00''$. The newly determined center of gravity is located at $\sim 7''$ southeast ($\Delta\alpha = 7.3^{\rm s}$, $\Delta\delta = -2''$) from that previously derived by Harris (1996) on the basis of the surface-brightness distribution.

In order to reduce spurious effects in the most crowded regions of the cluster, due to the low resolution of the WFI and *GALEX* observations, we considered only the *HST* data for the inner 85″ from the center, this value being imposed by the geometry of the combined WFPC2 FoVs (see Fig. 1). Thus, in the following, we define as the *HST sample* the ensemble of all the stars observed with *HST* at $r \leq 85''$ from $C_{\rm grav}$, and as the *External sample* all the stars detected with WFI and/or *GALEX* at $r > 85''$, out to $\sim 1100''$ (see Fig. 2). The CMDs of the *HST* and External samples in the (V, $B-V$) planes are shown in Figure 3.

Note that only the data suitable for the study of the BSS population is considered in the following, while those obtained through filters F160BW and FUV on board *HST* and *GALEX*, respectively, will be used in a forthcoming paper specifically devoted to the analysis of the HB properties (R. P. Schiavon et al. 2007, in preparation).

2.4. *Density Profile*

Considering all the stars brighter than $V = 20$ in the combined *HST* + External catalog (see Fig. 3), we have determined the projected density profile of NGC 1904 by direct star counts over

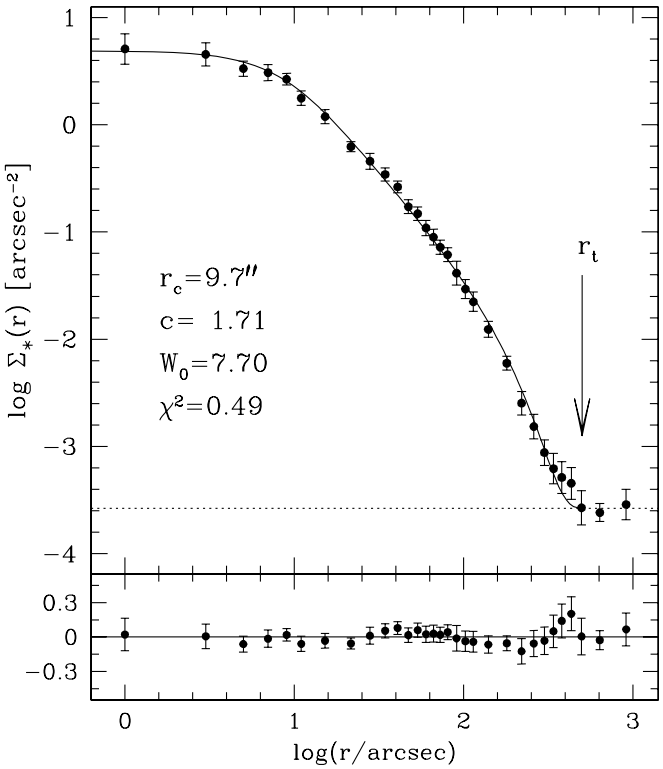


FIG. 4.—Observed surface density profile (*filled circles and error bars*) and best-fit King model (*solid line*). The radial profile is in units of number of stars per square arcsec. The dotted line indicates the adopted level of the background, and the model characteristic parameters (core radius r_c, concentration c, dimensionless central potential W_0), as well as the χ^2 value of the fit, are marked in the figure. The location of the cluster tidal radius is marked by the arrow. The lower panel shows the residuals between the observations and the fitted profile at each radial coordinate.

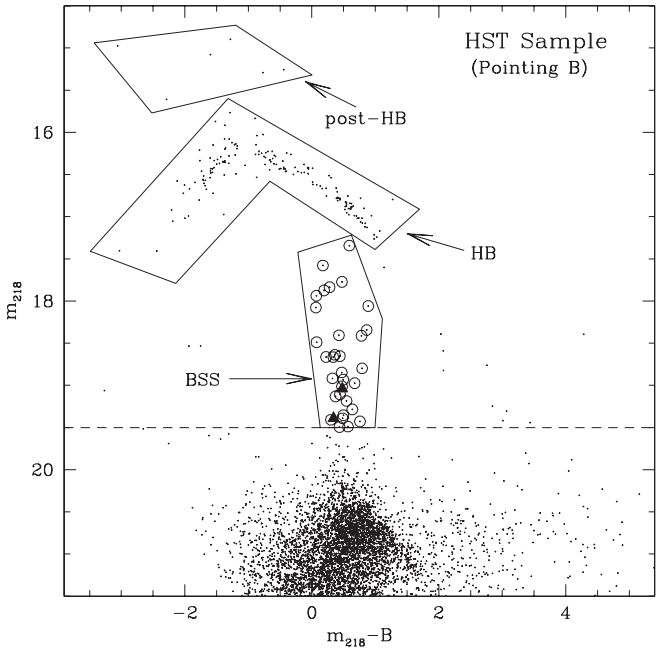


FIG. 5.—CMD of the ultraviolet (pointing B) *HST* sample. The adopted magnitude limit and selection box used for the definition of the BSS population (*open circles*) are shown. The two filled triangles correspond to BSS-38 and BSS-39, found in the External sample, with UV magnitudes obtained through the *GALEX* NUV detector. The selection boxes adopted for HB and post-HB stars are also shown.

the entire cluster extension. Following the procedure already described in Ferraro et al. (1999b, 2004), we have divided the entire sample into 31 concentric annuli, each centered on $C_{\rm grav}$ and split in an adequate number of subsectors (quadrants for the annuli totally sampled by the observations, octants elsewhere). The number of stars lying within each subsector was counted, and the star density was obtained by dividing these values by the corresponding subsector areas. The stellar density in each annulus was then obtained as the average of the subsector densities, and the standard deviation was estimated from the variance among the subsectors.

The radial density profile thus derived is plotted in Figure 4, and the average of the three outermost ($r > 8.3'$) surface density measures has been adopted as the background contribution (corresponding to 0.95 arcmin^{-2}). Figure 4 also shows the monomass King model that best fits the derived density profile, with the corresponding values of the core radius and concentration being $r_c \simeq 9.7''$ (with a typical error of $\sim\pm 2''$) and $c = 1.71$, respectively (hence, the tidal radius is $r_t \simeq 500'' \simeq 50 r_c$). These values are in good agreement with those quoted by Harris (1996; $r_c = 9.6''$ and $c = 1.72$), Trager et al. (1993; $r_c = 9.55''$ and $c = 1.72$), and McLaughlin & van der Marel (2005; $r_c = 10.3''$ and $c = 1.68$), derived from the surface-brightness profile, and they confirm that NGC 1904 has not yet experienced core collapse. By assuming a distance modulus $(m - M)_0 = 15.63$ (distance $d \sim 13.37$ kpc; Ferraro et al. 1999a), the derived value of r_c corresponds to $\sim$0.65 pc. By summing the luminosities of stars with $V \leq 20$ observed within $\sim 4''$, we estimate that the extinction-corrected central surface brightness of the cluster is $\mu_{V,0}(0) \simeq$ 16.20 mag arcsec^{-2}, in good agreement with Harris (1996; $\mu_{V,0} = 16.23$), Djorgovski (1993; $\mu_{V,0} = 16.15$), and McLaughlin & van der Marel (2005; $\mu_{V,0} = 16.18$). Following the procedure described in Djorgovski (1993; see also Beccari et al. 2006), we derive $\log \nu_0 \simeq 3.97$, where ν_0 is the central luminosity density in units of $L_\odot$ pc^{-3} (for comparison, $\log \nu_0 = 4.0$ in Harris 1996; Djorgovski 1993; McLaughlin & van der Marel 2005).

3. THE BSS POPULATION OF NGC 1904

3.1. *BSS Selection*

At UV wavelengths, BSSs are among the brightest objects in a GC, and RGB stars are particularly faint. By combining these advantages with the high-resolution capability of *HST*, the usual problems associated with photometric blends and crowding in the high-density central regions of GCs are minimized, and BSSs can be most reliably recognized and separated from the other populations in the UV CMDs. For these reasons, our primary criterion for the definition of the BSS sample is based on the position of stars in the $(m_{218},\ m_{218} - B)$ plane (see also Ferraro et al. 2004 for a detailed discussion of this issue). In order to avoid incompleteness bias and the possible contamination from TO and subgiant branch stars, we have adopted a limiting magnitude $m_{218} = 19.5$, roughly corresponding to 1 mag brighter than the cluster TO. The resulting BSS selection box in the UV CMD is shown in Figure 5. Once selected in the UV CMD, all the BSSs lying in the field in common with the optical-*HST* sample have been used to define the selection box in the $(V,\ B - V)$ and $(V,\ U - V)$ planes. The limiting magnitude in the V band is $V \simeq 18.9$, and the adopted BSS selection boxes in these planes are shown in Figures 3 and 6 (only stars not observed in *HST* pointing B are shown in the latter).

With these criteria, we have identified 39 BSSs in NGC 1904: 37 in the *HST* sample (32 from *HST* pointing B, and 5 from *HST* pointing A) and 2 in the External sample ($r > 85''$), the most

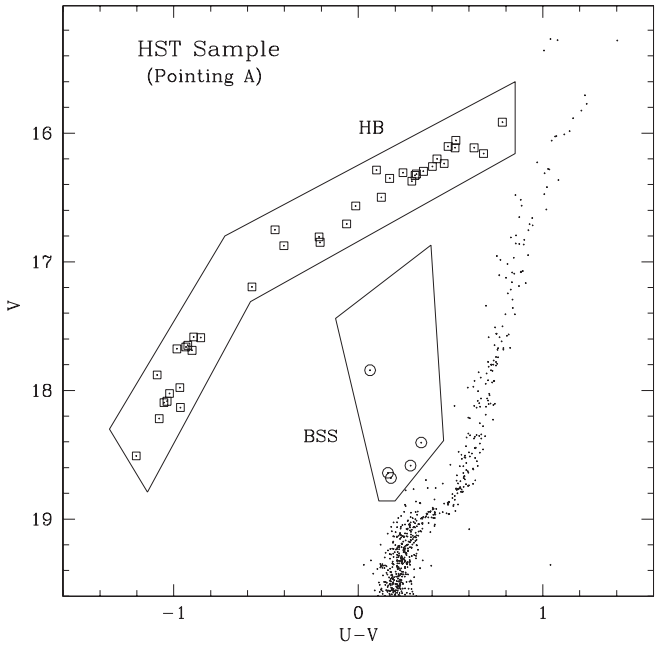


FIG. 6.—(V, $U-V$) CMD of the *HST* (pointing A) sample (only stars not observed in pointing B are plotted). The adopted BSS and HB selection boxes are shown, and all the identified BSSs and HB stars are marked with open circles and squares, respectively.

distant lying at $r \simeq 270''$ ($\sim 4.5'$) from the cluster center (see Fig. 2). All candidate BSSs have been confirmed by visual inspection, evaluating the quality and the precision of the PSF fitting. This procedure significantly reduces the possibility of introducing spurious objects, such as blends, background galaxies, etc., in the sample. The coordinates and magnitudes of all the identified BSSs are listed in Table 1.

In order to study the radial distribution of BSSs, one needs to compare their number counts as a function of radius with those of a population assumed to trace the radial density distribution of normal cluster stars. We chose to use HB stars for that purpose, given their high luminosities and relatively large number. Thanks to the (essentially blue) HB morphology, such a population can be easily selected in all CMDs, and the adopted selection boxes, designed to include the bulk of HB and the few post-HB stars, are shown in Figures 5–6. In order to be conservative, a few stars lying within the adopted HB selection boxes in the optical bands, but not detected in the UV filters (*GALEX*/NUV channel and *HST*/F218W filter), have been excluded from the following analysis. However, slightly different boxes or the inclusion of these stars in the sample have no effects on the results. With these criteria, we have identified 249 HB stars (197 at $r \leq 85''$ from the *HST* sample, and 52 at $85'' < r \leq r_t$ from the External sample).

3.2. *BSS Mass Distribution*

The positions of BSSs in the CMD can be used to derive a "photometric" estimate of their masses through the comparison with theoretical isochrones. We did this in the (V, $B-V$) plane, where 34 BSSs (32 from the *HST* pointing B and 2 from the External sample) out of the 39 identified in the cluster have been measured.

A set of isochrones of appropriate metallicity ($Z = 6 \times 10^{-4}$) has been extracted from the database of Cariulo et al. (2003) and transformed into the observational plane by adopting a reddening $E(B-V) = 0.01$ (Ferraro et al. 1999a). The 12 Gyr isochrone nicely reproduces the main cluster population, while the region of the CMD populated by the BSSs is well spanned by a set of isochrones with ages ranging from 1 to 6 Gyr (see Fig. 7). Thus, the entire data set of isochrones available in this age range (stepped at 0.5 Gyr) has been used to derive a grid linking the BSS colors and magnitudes to their masses. Each BSS has been projected on the closest isochrone, and a value of its mass has been derived. As shown in the lower panel of Figure 7, BSS masses range from ~ 0.95 to $\sim 1.6\, M_{\odot}$, and both the mean and the median of distribution correspond to $1.2\, M_{\odot}$. The TO mass turns out to be $M_{\rm TO} = 0.8\, M_{\odot}$.

3.3. *The BSS Radial Distribution*

The radial distribution of BSSs identified in NGC 1904 has been studied following the same procedure previously adopted for other clusters (see references in Ferraro 2006; Beccari et al. 2006). In Figure 8, we compare the BSS cumulative radial distribution to that of HB stars. The two distributions are obviously different, with the BSSs being more centrally concentrated than HB stars. A Kolmogorov-Smirnov test gives a $\sim 7 \times 10^{-4}$ probability that they are extracted from the same population, i.e., the two populations are different at more than the 3 σ level.

For a more quantitative analysis, the surveyed area has been divided into six concentric annuli, the first roughly corresponding to the core radius ($r = 10''$), and the others chosen in order to sample approximately the same fraction of the cluster luminosity out to the tidal radius ($r_t \simeq 500''$). The luminosity in each annulus has been calculated by integrating the surface density profile shown in Figure 4.

The number of BSSs and HB stars ($N_{\rm BSS}$ and $N_{\rm HB}$, respectively), as well as the fraction of sampled luminosity ($L^{\rm samp}$) measured in each annulus are listed in Table 2 and have been used to compute the population ratio $N_{\rm BSS}/N_{\rm HB}$ and the specific frequencies (see Ferraro et al. 2003):

$$R_{\rm pop} = \frac{(N_{\rm pop}/N_{\rm pop}^{\rm tot})}{(L^{\rm samp}/L_{\rm tot}^{\rm samp})}, \qquad (1)$$

with pop = BSS or HB.

The resulting radial trend of $R_{\rm HB}$ over the surveyed area is essentially constant, with a value close to unity (see Fig. 9). This is just what is expected on the basis of stellar evolution theory, which predicts that the fraction of stars in any post-main-sequence evolutionary stage is strictly proportional to the fraction of the sampled luminosity (Renzini & Fusi Pecci 1988). In contrast, the BSSs show a completely different radial distribution: as shown in Figure 9, the specific frequency, $R_{\rm BSS}$, is highly peaked at the cluster center, decreases to a minimum at $r \simeq 12 r_c$, and remains approximately constant outwards. The same behavior is clearly visible also in Figure 10, where the population ratio $N_{\rm BSS}/N_{\rm HB}$ is plotted as a function of r/r_c.

3.4. *Dynamical Simulations*

Following the same approach as Mapelli et al. (2004, 2006) and Lanzoni et al. (2007), we have used a Monte Carlo simulation code (originally developed by Sigurdsson & Phinney 1995) in order to reproduce the observed radial distribution and to derive some clues about the BSS formation mechanisms. Such a code follows the dynamical evolution of N BSSs within a background cluster, taking into account the effects of both dynamical friction and distant encounters. Since stellar collisions are most probable in the central high-density regions of the clusters, in the simulations, we define as COL-BSSs those objects with initial positions $r_i \lesssim r_c$. Since primordial binaries most likely evolve in

TABLE 1
THE BSS POPULATION IN NGC 1904

Name	R.A. (deg)	Decl. (deg)	m_{218}	U	B	V	I
BSS-1	81.048797100	−24.526391100	19.11	18.64	18.66	18.45	...
BSS-2	81.047782800	−24.526527400	18.65	18.12	18.21	17.94	...
BSS-3	81.047540400	−24.526005300	18.85	18.34	18.38	18.22	...
BSS-4	81.048954000	−24.525188200	17.94	17.75	17.87	17.78	...
BSS-5	81.047199200	−24.525797600	17.58	17.47	17.40	17.35	...
BSS-6	81.045528300	−24.525876800	18.64	18.24	18.28	18.12	...
BSS-7	81.044296100	−24.526362200	19.13	18.77	18.76	18.55	...
BSS-8	81.048506700	−24.524266800	19.18	18.55	18.64	18.39	...
BSS-9	81.041556100	−24.526972400	19.35	18.65	18.86	18.49	...
BSS-10	81.045827300	−24.525062700	18.06	17.35	17.17	16.96	...
BSS-11	81.045467700	−24.525147900	17.84	17.44	17.56	17.41	...
BSS-12	81.047088300	−24.524375900	18.80	18.20	18.01	17.80	...
BSS-13	81.046548400	−24.524483700	19.43	18.77	18.67	18.38	...
BSS-14	81.045121300	−24.524748300	19.28	18.33	18.65	18.21	...
BSS-15	81.045883300	−24.524278600	18.97	18.42	18.30	18.13	...
BSS-16	81.046164500	−24.522567300	18.41	17.72	17.63	17.42	...
BSS-17	81.044313700	−24.523304200	18.66	18.46	18.44	18.27	...
BSS-18	81.047157500	−24.521982700	18.49	18.45	18.41	18.32	...
BSS-19	81.043418100	−24.523247200	17.88	18.16	17.68	17.55	...
BSS-20	81.046665900	−24.520192000	19.49	18.71	18.92	18.60	...
BSS-21	81.044991400	−24.520127500	18.93	18.45	18.44	18.21	...
BSS-22	81.046157800	−24.519245100	19.49	18.92	19.06	18.74	...
BSS-23	81.049326100	−24.521621900	18.08	...	18.01	17.99	...
BSS-24	81.049155900	−24.520629500	18.41	...	17.98	17.87	...
BSS-25	81.047244500	−24.517052600	19.41	18.97	19.11	18.82	...
BSS-26	81.051592200	−24.523146600	18.67	...	18.33	18.21	...
BSS-27	81.050476100	−24.517107000	19.01	18.65	18.54	18.39	...
BSS-28	81.060767000	−24.520983900	18.92	...	18.59	18.45	...
BSS-29	81.068117100	−24.517558600	19.39	...	18.91	18.60	...
BSS-30	81.043233100	−24.533852000	17.34	...	16.75	16.65	...
BSS-31	81.044917900	−24.540315000	18.34	...	17.48	17.22	...
BSS-32	81.038520800	−24.540891600	17.77	17.46	17.30	17.20	...
BSS-33	81.045196533	−24.515874863	...	17.91	...	17.84	...
BSS-34	81.032196045	−24.512256622	...	18.75	...	18.41	...
BSS-35	81.037574768	−24.525493622	...	18.87	...	18.58	...
BSS-36	81.041069031	−24.518457413	...	18.80	...	18.64	...
BSS-37	81.045227051	−24.517648697	...	18.86	...	18.68	...
BSS-38	81.056510925	−24.449676514	19.04[a]	18.78	18.56	18.35	18.08
BSS-39	81.058883667	−24.555763245	19.39[a]	19.14	19.05	18.73	18.34

[a] Note that while the header of the column refers to *HST*-F218W magnitudes, those of BSS-38 and BSS-39 have been obtained with the NUV channel of *GALEX* and transformed to the m_{218} scale, as described in § 2.2.

isolation if they orbit in the cluster outskirts, we identify as MT-BSSs those BSSs with $r_i \gg r_c$. Within these definitions, in any given run we assume that a certain fraction of the N simulated BSSs is made of COL-BSSs, and the remaining fraction of MT-BSSs. The initial positions r_i of the two types of BSS are randomly generated within the appropriate radial range ($r_i \lesssim r_c$ for COL-BSS, and $r_i \gg r_c$ for the others) following a flat distribution, according to the fact that the number of stars in a King model scales as $dN = n(r)\,dV \propto r^{-2}\pi r^2\,dr \propto dr$. Their initial velocities are randomly extracted from the cluster velocity distribution illustrated in Sigurdsson & Phinney (1995), and an additional natal kick is assigned to COL-BSSs to account for the recoil induced by the three-body encounters that trigger the merger and produce the BSSs (see, e.g., Sigurdsson et al. 1994; Davies et al. 1994). Each BSS has characteristic mass M and maximum lifetime $t_{\rm last}$. We follow their dynamical evolution in the (fixed) gravitational potential for a time t_i ($i = 1, N$), where each t_i is a randomly chosen fraction of $t_{\rm last}$. At the end of the simulation, we register the final positions of the BSSs, and we compare their radial distribution with the observed one. The percentage of COL- and MT-BSSs is changed and the procedure repeated until a reasonable agreement between the simulated and the observed distributions is reached.

For a more detailed discussion of the procedure and the ranges of values appropriate for the input parameters, we refer to Mapelli et al. (2006). Here we only list the assumptions made in the present study:

1. The background cluster has been approximated with a multimass King model, determined as the best fit to the observed profile.[14] The cluster central velocity dispersion is set to $\sigma = 3.9$ km s^{-1} (Dubath et al. 1997), and assuming 0.5 $M_\odot$ as the average mass of the cluster stars, the central stellar density is $n_c = 3 \times 10^4$ pc^{-3} (Pryor & Meylan 1993).
2. BSS masses have been fixed to $M = 1.2\ M_\odot$ (see § 3.2), and characteristic lifetimes $t_{\rm last}$ ranging between 1.5 and 4 Gyr have been considered.

[14] By adopting the same mass groups as those of Mapelli et al. (2006), the resulting value of the King dimensionless central potential is $W_0 = 10$.

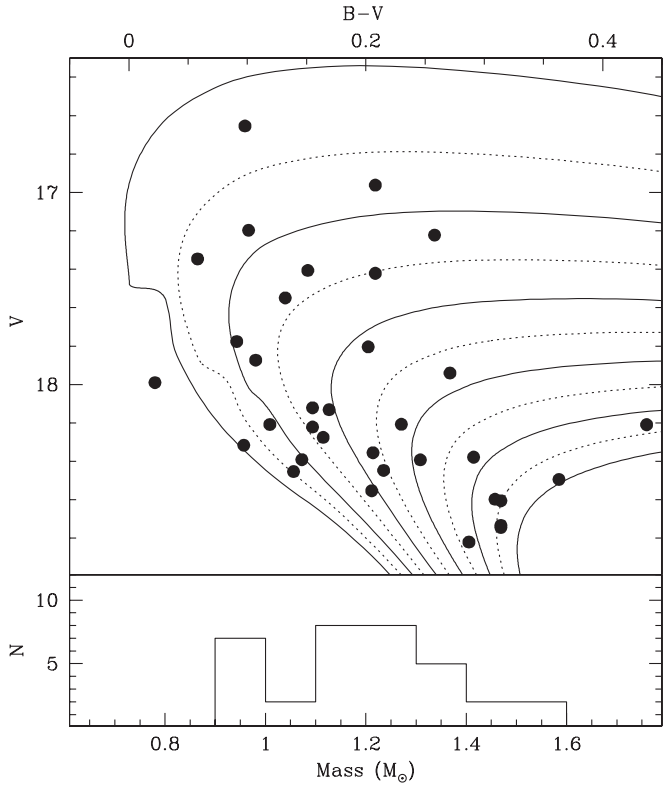


FIG. 7.—*Upper panel*: Zoomed (V, $B-V$) CMD of the BSS region; the 34 BSSs measured in this plane are shown. The set of isochrones ranging from 1 to 6 Gyr (stepped by 0.5 Gyr) from the Cariulo et al. (2003) database used to derive BSS masses is also shown. *Lower panel*: Derived mass distribution for the BSSs shown in the upper panel.

TABLE 2
BSS AND HB STAR NUMBER COUNTS IN NGC 1904

r_i	r_e	N_{BSS}	N_{HB}	L^{samp}/L^{samp}_{tot}
0.....	10	15	34	0.14
10.....	20	10	45	0.18
20.....	40	7	62	0.22
40.....	85	5	56	0.23
85.....	150	1	34	0.13
150.....	500	1	18	0.10

NOTES.—Number of BSS and HB stars and fraction of luminosity sampled in the six concentric annuli used to study the BSS radial distribution of NGC 1904 (r_i and r_e correspond to the internal and external radius of each considered annulus, in arcsec).

3. COL-BSSs have been distributed with initial positions $r_i \leq r_c$ and have been given a natal kick velocity of 1 σ.
4. Initial positions ranging between $5r_c$ and r_t have been considered for MT-BSSs in different runs.
5. In each simulation, we have followed the evolution of $N = 10{,}000$ BSSs.

The simulated radial distribution that best reproduces the observed one (with a reduced $\chi^2 \simeq 0.1$) is shown in Figure 10 and is obtained by assuming that the totality of BSSs is made of COL-BSSs. In the best-fit case, the BSS characteristic lifetime is $t_{last} \simeq 1.5$ Gyr, but a variation between 1 and 4 Gyr of this parameter still leads to a very good agreement ($\chi^2 \simeq 0.2$–0.3) with the observations. For the sake of comparison, in Figure 10 we also show the results of the simulations obtained by assuming a percentage of MT-BSSs ranging from 10% to 40% (see lower and upper boundaries of the gray region, respectively).[15] As

[15] Note that a population of 40% MT-BSSs was needed in order to reproduce the bimodal distribution observed in M3, 47 Tuc, and NGC 6752 (Mapelli et al. 2006), and 10% was found to be the appropriate percentage of MT-BSSs in the case of M5 (Lanzoni et al. 2007).

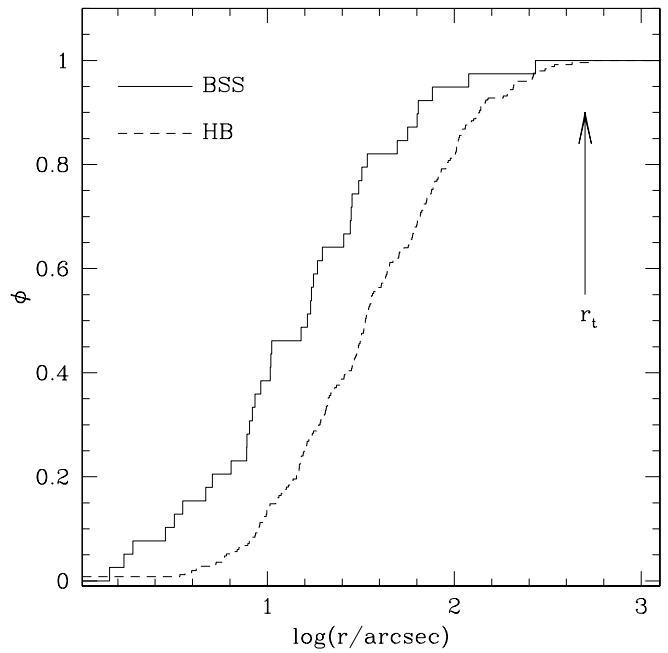


FIG. 8.—Cumulative radial distribution of BSSs (*solid line*) and HB stars (*dashed line*) as a function of the projected distance from the cluster center for the combined *HST* + External sample. The location of the cluster tidal radius is marked by the arrow.

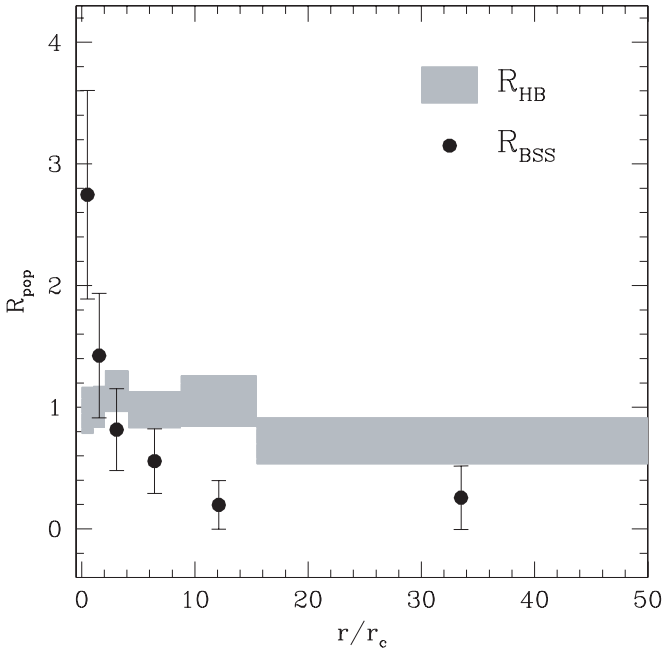


FIG. 9.—Radial distribution of the BSS (*circles*) and HB (*gray regions*) specific frequencies, as defined in eq. (1), and as a function of the radial distance in units of the core radius. The vertical size of the gray regions correspond to the error bars.

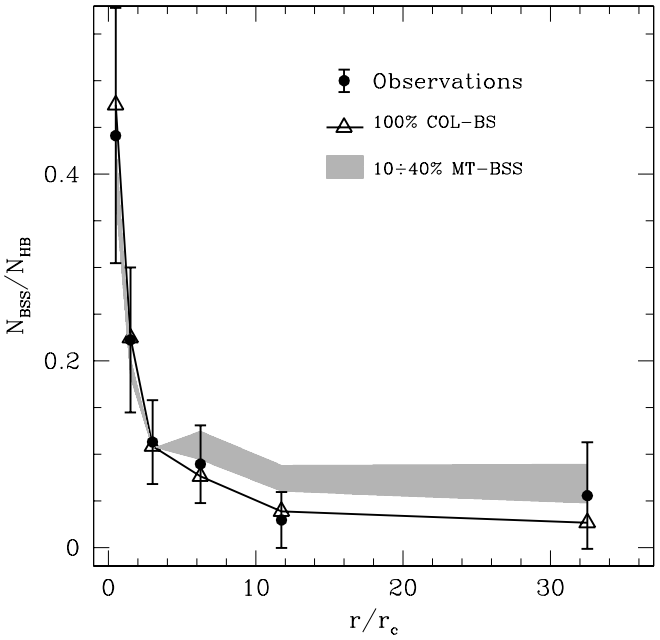


FIG. 10.— Radial distribution of the population ratio N_{BSS}/N_{HB} as a function of r/r_c (*circles with error bars*), compared to the simulated distribution (*solid line and triangles*) obtained by assuming 100% of COL-BSSs. The results of the simulations obtained by assuming a percentage of MT-BSSs ranging from 10% to 40% (*lower and upper boundaries of the gray region, respectively*) are also shown.

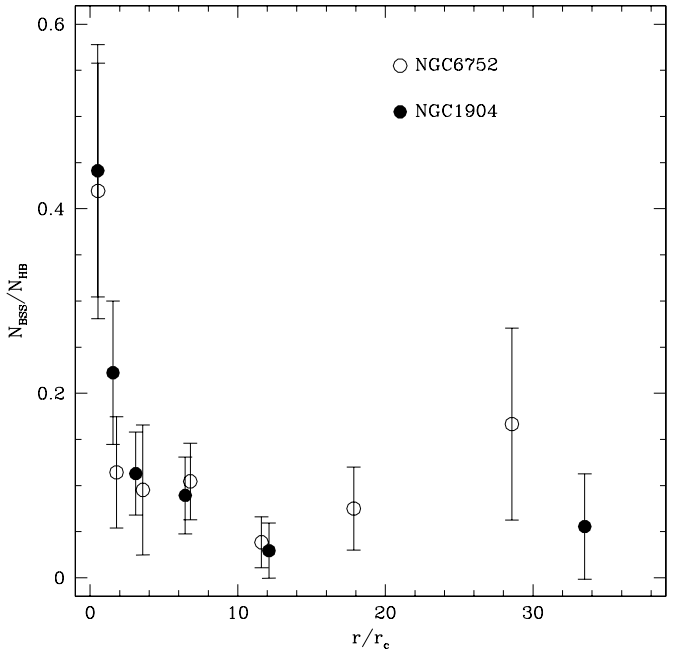


FIG. 11.— Radial distribution of the population ratio N_{BSS}/N_{HB} for NGC 1904 (*filled circles*) and NGC 6752 (*open circles*) plotted as a function of the radial distance in core radius units.

can be seen, while a population of 10% MT-BSSs is still marginally consistent with the observations, larger percentages systematically overestimate the BSS population at $r \gtrsim 5r_c$. Increasing the BSS mass up to 1.5 $M_\odot$ does not change this conclusion.

By assuming 12 Gyr for the age of NGC 1904, we have used the simulations and the dynamical friction timescale (from, e.g., Mapelli et al. 2006) for 1.2 $M_\odot$ stars to estimate the radius of avoidance r_{avoid} of the cluster, i.e., the radius within which all these stars are expected to have already sunk to the cluster core because of mass segregation processes. We find that $r_{avoid} \sim 30r_c$ (i.e., $\sim 300''$), which corresponds to a significant fraction of the entire cluster extension. This evidence is consistent with the fact that the simulated MT-BSSs appear to be a negligible fraction of the overall BSS population.

4. DISCUSSION

We have studied the brightest portion ($m_{218} \leq 19.5$) of the BSS population in NGC 1904. We have found a total of 39 objects, with a high degree of segregation in the cluster center. Approximately 38% of the entire BSS population is found within the cluster core, while only $\sim$13% of HB stars are counted in the same region. This indicates a significant overabundance of BSSs in the center, as also confirmed by the fact that the BSS specific frequency R_{BSS} within r_c is roughly 3 times larger than expected for a normal (nonsegregated) population on the basis of the sampled light (see Fig. 9). The peak value is in good agreement with what is found in the case of M3, 47 Tuc, NGC 6752, and M5 (see Ferraro et al. 2004; Sabbi et al. 2004; Lanzoni et al. 2007). Unlike these clusters, no significant upturn of the distribution at large radii has been detected in NGC 1904.

We emphasize that the absence of an external upturn in the BSS radial distribution is not an effect of low statistics. In the case of NGC 6752, where a similar number of BSSs (34) has been detected, the BSS radial distribution is clearly bimodal (Sabbi et al. 2004). This can also be seen in Figure 11, where the two distributions are directly compared. They nicely agree within $r \sim 12r_c$, but the fraction of BSSs in NGC 6752 rises again at larger distances from the center, despite the smaller number of BSSs observed in this cluster, compared to NGC 1904.

Extensive dynamical simulations have been used to derive some hints about the BSS formation mechanisms. Even if admittedly crude, this approach has been successfully used to demonstrate that the external rising branch of the BSS radial distribution observed in M3, 47 Tuc, NGC 6752, and M5 cannot be due to COL-BSSs originating in the core and then being kicked out in the outer regions; hence, a significant fraction (20%–40%) of the overall population in these clusters must consist of MT-BSSs (Mapelli et al. 2006; Lanzoni et al. 2007). By using the same simulations to interpret the (flat) BSS radial distribution of NGC 1904, we found that only a negligible percentage (0%–10%) of MT-BSSs is needed. However, we emphasize that if a rising peripheral BSS frequency is absent (as in the case of NGC 1904), our simple approach cannot distinguish between BSSs created by MT (and then segregated into the cluster core by the dynamical friction) and COL-BSSs created by collisions inside the core.

On the other hand, the negligible fraction of peripheral MT-BSSs found in NGC 1904 is in agreement with the quite large value of the radius of avoidance estimated for this cluster ($r_{avoid} \simeq 30r_c$), which indicates that all the heavy stars (binaries) within this radial distance have had enough time to sink to the core and are therefore not expected in the cluster outskirts. Such a radial distance corresponds to $0.6r_t$, i.e., it represents a significant fraction of the cluster extension (only 1% of the cluster light is contained between r_{avoid} and r_t), and hence only a small fraction of the massive objects are expected to be unaffected by the dynamical friction. In all the other studied cases, r_{avoid} is significantly smaller: $r_{avoid} \lesssim 0.2r_t$ (Mapelli et al. 2006; Lanzoni et al. 2007). In turn, this suggests that at least a fraction of the BSS population that we now observe in the cluster center are primordial

binaries which have sunk to the core because of the dynamical friction process and mixed with those that formed through stellar collisions. Only systematic surveys of physical and chemical properties for a large number of BSSs in different environments (see examples in De Marco et al. 2005; Ferraro et al. 2006b) can definitively identify the formation processes of these stars.

This research was supported by Agenzia Spaziale Italiana under contract ASI-INAF I/023/05/0, by the Istituto Nazionale di Astrofisica under contract PRIN/INAF 2006, and by the Ministero dell'Istruzione, dell'Università e della Ricerca. R. T. R. is partially funded by NASA through grant HST-GO-10524 from the Space Telescope Science Institute.

REFERENCES

Bailyn, C. D. 1995, ARA&A, 33, 133
Bailyn, C. D., & Pinsonneault, M. H. 1995, ApJ, 439, 705
Beccari, G., Ferraro, F. R., Lanzoni, B., & Bellazzini, M. 2006, ApJ, 652, L121
Buonanno, R., Buscema, G., Corsi, C. E., Ferraro, I., & Iannicola, G. 1983, A&A, 126, 278
Buonanno, R., & Iannicola, G. 1989, PASP, 101, 294
Cariulo, P., Degl'Innocenti, S., & Castellani, V., 2004, A&A, 421, 1121
Carney, B. W., Latham, D. W., & Laird, J. B. 2005, AJ, 129, 466
Davies, M. B., Benz, W., & Hills, J. G. 1994, ApJ, 424, 870
De Marco, O., Shara, M. M., Zurek, D., Ouellette, J. A., Lanz, T., Saffer, R. A., & Sepinsky, J. F. 2005, ApJ, 632, 894
Djorgovski, S. 1993, in ASP Conf. Ser. 50, Structure and Dynamics of Globular Clusters, ed. S. G. Djorgovski & G. Meylan (San Francisco: ASP), 373
Dorman, B., O'Connell, R. W., & Rood, R. T. 1995, ApJ, 442, 105
Dubath, P., Meylan, G., & Mayor, M. 1997, A&A, 324, 505
Ferraro, F. R. 2006, preprint (astro-ph/0601217)
Ferraro, F. R., Beccari, G., Rood, R. T., Bellazzini, M., Sills, A., & Sabbi, E. 2004, ApJ, 603, 127
Ferraro, F. R., Clementini, G., Fusi Pecci, F., Sortino, R., & Buonanno, R. 1992, MNRAS, 256, 391
Ferraro, F. R., D'Amico, N., Possenti, A., Mignani, R. P., & Paltrinieri, B. 2001, ApJ, 561, 337
Ferraro, F. R., Messineo, M., Fusi Pecci, F., De Palo, M. A., Straniero, O., Chieffi, A., & Limongi, M. 1999a, AJ, 118, 1738
Ferraro, F. R., Paltrinieri, B., Fusi Pecci, F., Cacciari, C., Dorman, B., Rood, R. T., Buonanno, R., Corsi, C. E., Burgarella, D., & Laget, M. 1997, A&A, 324, 915
Ferraro, F. R., Paltrinieri, B., Rood, R. T., & Dorman, B. 1999b, ApJ, 522, 983
Ferraro, F. R., Sills, A., Rood, R. T., Paltrinieri, B., & Buonanno, R. 2003, ApJ, 588, 464
Ferraro, F. R., Sollima, A., Rood, R. T., Origlia, L., Pancino, E., & Bellazzini, M. 2006a, ApJ, 638, 433
Ferraro, F. R., et al. 2006b, ApJ, 647, L53
Harris, W. E. 1996, AJ, 112, 1487
Holtzman, J. A., Burrows, C. J., Casertano, S., Hester, J. J., Trauger, J. T., Watson, A. M., & Worthey, G. 1995, PASP, 107, 1065
Kravtsov, V., Ipatov, A., Samus, N., Smirnov, O., Alcaino, G., Liller, W., & Alvarado, F. 1997, A&AS, 125, 1
Lanzoni, B., Dalessandro, E., Ferraro, F. R., Mancini, C., Beccari, G., Rood, R. T., Mapelli, M., & Sigurdsson, S. 2007, ApJ, in press
Leigh, N., Sills, A., & Knigge, C. 2007, ApJ, 661, 210
Mapelli, M., Sigurdsson, S., Colpi, M., Ferraro, F. R., Possenti, A., Rood, R. T., Sills, A., & Beccari, G. 2004, ApJ, 605, L29
Mapelli, M., Sigurdsson, S., Ferraro, F. R., Colpi, M., Possenti, A., & Lanzoni, B. 2006, MNRAS, 373, 361
Mateo, M., Harris, H. C., Nemec, J., & Olszewski, E. W. 1990, AJ, 100, 469
McLaughlin, D. E., & van der Marel, R. P. 2005, ApJS, 161, 304
Montegriffo, P., Ferraro, F. R., Fusi Pecci, F., & Origlia, L. 1995, MNRAS, 276, 739
Pritchet, C. J., & Glaspey, J. W. 1991, ApJ, 373, 105
Pryor, C., & Meylan, G. 1993, in ASP Conf. Ser. 50, Structure and Dynamics of Globular Clusters, ed. S. G. Djorgovski & G. Meylan (San Francisco: ASP), 357
Renzini, A., & Fusi Pecci, F. 1988, ARA&A, 26, 199
Sabbi, E., Ferraro, F. R., Sills, A., & Rood, R. T. 2004, ApJ, 617, 1296
Shara, M. M., Saffer, R. A., & Livio, M. 1997, ApJ, 489, L59
Sigurdsson, S., Davies, M. B., & Bolte, M. 1994, ApJ, 431, L115
Sigurdsson, S., & Phinney, E. S. 1995, ApJS, 99, 609
Stetson, P. B. 1987, PASP, 99, 191
———. 2000, PASP, 112, 925
Tian, B., Deng, L., Han, Z., & Zhang, X. B. 2006, A&A, 455, 247
Trager, S. C., Djorgovski, S., & King, I. R. 1993, ASP Conf. Ser. 50, Structure and Dynamics of Globular Clusters, ed. S. G. Djorgovski & G. Meylan (San Francisco: ASP), 347
Warren, S. R., Sandquist, E. L., & Bolte, M. 2006, ApJ, 648, 1026
Zaggia, S. R., Piotto, G., & Capaccioli, M. 1997, A&A, 327, 1004